

UbiHR: Resource-efficient Long-range Heart Rate Sensing on Ubiquitous Devices

HAOYU BIAN, Northwestern Polytechnical University, China

BIN GUO, Northwestern Polytechnical University, China

SICONG LIU, Northwestern Polytechnical University, China

YASAN DING, Northwestern Polytechnical University, China

SHANSHAN GAO, Hospital of Xi'an Jiaotong University, China

ZHIWEN YU, Northwestern Polytechnical University, Harbin Engineering University, China

Ubiquitous on-device heart rate sensing is vital for high-stress individuals and chronic patients. Non-contact sensing, compared to contact-based tools, allows for natural user monitoring, potentially enabling more accurate and holistic data collection. However, in open and uncontrolled mobile environments, user movement and lighting introduce noises. Existing methods, such as curve-based or short-range deep learning recognition based on adjacent frames, strike the optimal balance between real-time performance and accuracy, especially under limited device resources. In this paper, we present UbiHR, a ubiquitous device-based heart rate sensing system. Key to UbiHR is a real-time long-range spatio-temporal model enabling noise-independent heart rate recognition and display on commodity mobile devices, along with a set of mechanisms for prompt and energy-efficient sampling and preprocessing. Diverse experiments and user studies involving four devices, four tasks, and 80 participants demonstrate UbiHR's superior performance, enhancing accuracy by up to 74.2% and reducing latency by 51.2%.

CCS Concepts: • **Human-centered computing** → **Ubiquitous and mobile computing**; • **Computing methodologies** → **Machine learning**.

Additional Key Words and Phrases: Long-range Spatio-temporal Sensing

ACM Reference Format:

Haoyu Bian, Bin Guo, Sicong Liu, Yasan Ding, Shanshan Gao, and Zhiwen Yu. May2024. UbiHR: Resource-efficient Long-range Heart Rate Sensing on Ubiquitous Devices. *Proc. ACM Interact. Mob. Wearable Ubiquitous Technol.* 1, 1 (October May2024), 26 pages. <https://doi.org/11.1111/11111111>

1 INTRODUCTION

Physiological health sensing anytime and anywhere is important for users, encompassing metrics like heart rate [23, 60], blood oxygen [25], blood pressure [24], etc. Existing methods include hospital-grade and consumer-grade solutions, both contact-based and non-contact. However, discomfort is a common issue with contact-based options like specialized vests [38] and fingertip monitors [29], while wearable devices such as watches [36],

Corresponding author: Bin Guo(guob@nwpu.edu.cn), Sicong Liu(scliu@nwpu.edu.cn).

Authors' addresses: [Haoyu Bian](#), Northwestern Polytechnical University, School of Computer Science, Xi'an, China; [Bin Guo](#), Northwestern Polytechnical University, School of Computer Science, Xi'an, China; [Sicong Liu](#), Northwestern Polytechnical University, School of Computer Science, Xi'an, China; [Yasan Ding](#), Northwestern Polytechnical University, School of Computer Science, Xi'an, China; [Shanshan Gao](#), Hospital of Xi'an Jiaotong University, Department of Cardiovascular Medicine, Xi'an, China; [Zhiwen Yu](#), Northwestern Polytechnical University, Harbin Engineering University, School of Computer Science, Harbin, China.

Permission to make digital or hard copies of all or part of this work for personal or classroom use is granted without fee provided that copies are not made or distributed for profit or commercial advantage and that copies bear this notice and the full citation on the first page. Copyrights for components of this work owned by others than the author(s) must be honored. Abstracting with credit is permitted. To copy otherwise, or republish, or post on servers or to redistribute to lists, requires prior specific permission and/or a fee. Request permissions from permissions@acm.org.

© May2024 Copyright held by the owner/author(s). Publication rights licensed to ACM.

ACM 2474-9567/May2024/10-ART

<https://doi.org/11.1111/11111111>

wristbands worn on the wrist [3, 9, 75], and glasses [13] impose limitations by compressing the skin and affecting daily activities. There is a need for a *ubiquitous, non-contact* heart rate sensing tool utilizing mobile and embedded cameras. This allows for user monitoring in *natural settings*, leading to potentially more accurate and holistic data collection. For instance, camera-based heart rate sensing can aid law enforcement in detecting truthfulness during confessions without awareness or psychological resistance, and enabling convenient health monitoring for elderly individuals living alone.

Meanwhile, the pervasive deployment of camera-embedded devices *e.g.*, smartphones, wearables, tablets, and robots has stimulated a wide spectrum of novel video-based physiological applications. Examples include Mobilephys on smartphones [52] and TS-CAN on embedded platforms [50]. Despite extensive research on camera-based heart rate sensing [11, 58, 74, 80, 83, 84], they are unfit for deployment to ubiquitous mobile and embedded devices because they fail to meet the following requirements.

- *Low-cost end-to-end* heart rate sensing on resource-constrained ubiquitous devices is non-trivial for practical applications. While video-based remote photoplethysmography (rPPG) measurements are commonly used for heart rate sensing, privacy concerns dictate *on-device preprocessing and processing* [45] instead of cloud streaming. However, enabling this capability on low-end mobile and embedded devices faces challenges due to high computing overhead. Previous studies rely on hand-crafted methods [11] or complex pre-processing techniques, such as retaining only the facial region of interest (RoI) through face detection [26], dividing the image into small blocks/channels [54, 72], or constructing a 3D model [44], assuming given pre-processed data. As demonstrated in Sec. 4, these methods struggle to realize high accuracy with low on-device latency.
- *Real-time* spatio-temporal heart rate sensing from noisy video streams poses a significant challenge. Unlike traditional analysis of signals acquired by contact-based devices, which focuses on prominent changes, facial rPPG measurement requires capturing subtle facial movements and color variations, complicating global spatial-temporal recognition. Also, adapting existing curve-based models, such as color space projection [6, 51] and skin reflection [76], to dynamic open environments (*e.g.*, various light conditions [49]) proves challenging, as none of them consider rPPG signal periodic properties in long-range sensing [84]. Factors such as user head motions, lighting fluctuations, and equipment noise further complicate the recognition process. Addressing these challenges necessitates intricate long-range and noise-robust spatio-temporal DL models, which are unsuitable for resource-constrained ubiquitous devices.

In this paper, we present UbiHR, a real-time and continuous *on-device* heart rate sensing system for ubiquitous mobile and embedded devices with *long-range* video streams. To ensure user-friendly design and reduce bias, we conduct pre-design surveys with 80 participants, including 30 students and 50 patients, to understand user demands. Achieving real-time and high-accuracy performance demand with non-stationary noisy videos on low-end resource-limited devices poses significant challenges. Our *key insight* is that detecting on long-range is more conducive to detecting the inherent periodic characteristics and trends of heart rate, enhancing the ability to resist environmental noise. Specifically, UbiHR incorporates three modules. *First*, an *adaptive duty-cycling facial video sampling* module dynamically switches between sleeping, short-term listening, and long-term listening schemes to balance energy consumption and promptness of facial key point detection. *Second*, a *dynamic noise-aware facial image pre-processing* module extracts essential facial key points through differentiation and normalization, eliminating noise from user head motion and varying environmental lighting conditions while reducing input volume for subsequent real-time processing. *Third*, a *fast long-range spatio-temporal heart rate recognizing* module integrates a zero-parameter time shift strategy into 2D convolution for lightweight spatio-temporal modeling. It extracts both long-range and short-range spatio-temporal features from the heart rate signal using parallel multi-branch structures and corrects accuracy using soft-attention masks.

We implement UbiHR as a python package that can be easily integrated into other applications on four typical mobile and embedded devices, *i.e.*, IQOO9 smart phone, Raspberry, Jetson orin, and Jetson AGX. We evaluate

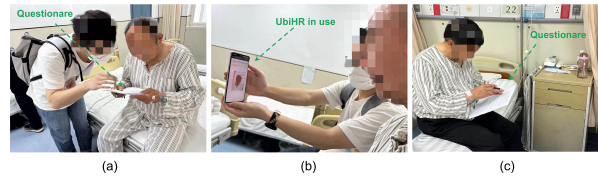


Fig. 1. Questionnaire survey on a hospital cardiology department and user experience of UbiHR.

the performance of UbiHR on four open datasets and real-world scenarios with diverse user motion or light conditions. Results show a reduction of up to 74.2% in recognizing error (*i.e.*, MAE, MAPE, RMSE), up to 51.2% in inference latency, 49% in memory cost, and 19% in energy cost. Especially, UbiHR achieves up to 42.8% accuracy increase in long-range video streams (Sec. 4.5). Our main contributions are summarized as follows:

- To the best of our knowledge, UbiHR is the first *real-time on-device* contactless heart rate sensing tool on ubiquitous devices with *long-range* video streams. It delivers real-time, high-accuracy video sampling, preprocessing, and processing on commodity platforms while maintaining robustness against various noise.
- We realize UbiHR as an end-to-end mobile system. The key technical novelties include adaptive duty-cycling facial video sampling, dynamic noise-aware facial image preprocessing, and fast long-range spatio-temporal heart rate recognizing.
- We evaluate UbiHR on 4 public benchmarks and real-world ubiquitous scenarios on four mobile platforms. Experiments show that UbiHR achieves near real-time (5.01 ~ 30.9 ms) with over 20.9% higher accuracy than state-of-the-art methods.

In the rest of this paper, we conduct a pre-design survey in Sec. 2, detail the system design in Sec. 3. We next present the system implementation and evaluate the system in Sec. 4. Finally, we review the related work in Sec. 5 and conclude in Sec. 6.

2 USER STUDY

To understand the needs and usage preferences of ubiquitous users regarding a camera-based heart rate sensing tool, we designed a questionnaire and distributed it to 80 users from our school and a hospital cardiology department. Participants' ages ranged from 20 to 76 years old, as shown in Fig. 1. Permission was obtained from both the hospital and participants, and the questionnaire included multiple-choice and open-ended questions.

2.1 Survey Findings

We briefly summarize the results (as shown in Fig. 2) of our survey as follows.

2.1.1 User Demands on Fast and Long-term Heart Rate Sensing. Through surveys, various groups of individuals require frequent and long-term heart rate sensing: *i)* Patients with cardiovascular, hypertension, and diabetes conditions need it to assess treatment effectiveness, evaluate blood pressure control, assess cardiovascular risk, and prevent complications. For instance, individuals with arrhythmia need continuous monitoring to assess treatment effectiveness, evaluate blood pressure control, assess cardiovascular risk, and prevent complications. Long-term heart rate sensing aids in the timely detection and treatment of potential heart issues, mitigating the risk of cardiac events, *e.g.*, **too fast** (ventricular tachycardia), **too slow** (high degree atrioventricular block), or **irregular** (paroxysmal atrial fibrillation). *ii)* Elderly users require it to assess cardiovascular health and promptly detect and manage potential issues. As people age, the risk of cardiovascular diseases in the elderly rises, making timely cardiovascular health assessments crucial. It helps doctors to timely perform further examinations and diagnoses, facilitating early detection and treatment of potential cardiovascular issues. *iii)* Athletes and fitness enthusiasts

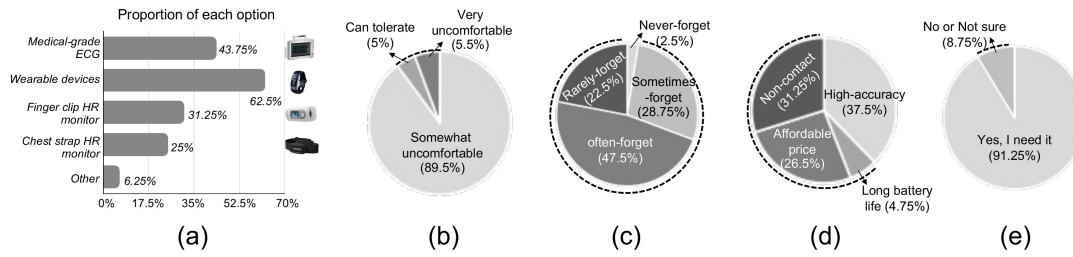


Fig. 2. Survey results: (a) What method(s) do you currently use to measure HR? (b) Do you feel uncomfortable with the HR measurement method(s) that require skin contact (such as wearing a chest strap or finger clip?) (c) Do you often forget to wear or use HR measurement devices that require skin contact? (d) What features would you like the tool to have? (e) Do you think there is a need for a contactless HR sensing tool in addition to your current HR measurement method(s)?

need it to continuously evaluate exercise intensity and optimize training plans to prevent overtraining. Unlike traditional methods, contactless heart rate monitoring eliminates the need for athletes to wear contact-based devices, ensuring their movements and performance during training remain unaffected. *iv*) Individuals managing stress and mental health benefit from continuous heart rate monitoring, as heart rate closely correlates with stress levels and emotional states. This is particularly important for young users experiencing high work stress who require continuous assessment of stress levels. This can boost users' self-awareness and motivate proactive relaxation and adjustment.

2.1.2 Limitations of existing heart rate sensing tools. The majority of participants currently depend on wearable devices and medical-grade electrocardiogram (ECG) equipment at hospitals, constituting 62.5% (50/80) and 43.75% (35/80), respectively. However, participants voiced concerns: 95% of participants expressed discomfort with ECGs attached to the chest or clipped to fingers. This suggests that current medical-grade, contact-based ECG equipment may not offer a comfortable user experience, potentially affecting user acceptance and long-term usage. Furthermore, 76.25% of participants admitted to frequently or occasionally forgetting to wear them, potentially compromising the long-term waiting time for health sensing. This compromises long-term data acquisition for health monitoring and detecting health trends or early warning signs.

2.1.3 Willingness to use contactless and ubiquitous heart rate sensing tools. 91.25% of participants expressed the need for an additional heart rate sensing tool in addition to their current use of devices attached to the chest or clipped to fingers. Moreover, the desired features for this tool include high measurement accuracy (37.5%) and a contactless sensing mode (31.25%) that does not require attachment to the chest or finger.

2.2 Design Goals

To further understand the requirements of the contactless heart rate sensing tool, we asked each participant to rate the importance of different performance aspects of the tool and summarized the results as our design goals.

- **On-device.** 60% of participants are unwilling to stream out their sensitive raw videos to the cloud for analysis. Thus, video stream collection and inference should be conducted locally on the device. Additionally, 70% of participants prefer interacting with local devices over the cloud to protect sensitive data privacy and reduce network dependency.
- **Accurate.** 80% of participants reported low tolerance for errors, and 63% of participants can only tolerate a maximum error of 5 times in terms of bmp (heart rate beats per minute).
- **Responsive.** 70% of participants are comfortable receiving results within 30ms of detection initiation. Heart rate sensing and recognition should offer *real-time performance* and prompt user notifications.

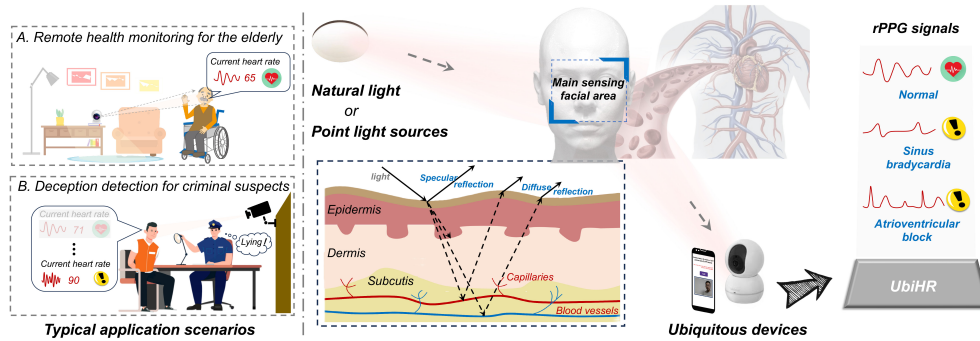


Fig. 3. Illustration of the principle of mapping cardio-pulmonary and facial signal for contactless heart rate sensing.

- *Energy-efficient.* Over 85% of participants expressed concerns about the energy consumption of the tool on battery-powered ubiquitous devices, such as smartphones. It should enable *continuous sensing* with minimal energy cost.

2.3 Why Camera-based Physiological Sensing

Cameras can detect physiological signals by capturing facial videos, including heart rate, respiration rate, and blood oxygen saturation [66]. This capability relies on the principle of contactless cardiopulmonary measurement, which involves detecting subtle changes in the reflected light from the body resulting from physiological processes. As shown in Figure 3, biologically, when blood volume increases (such as during each heartbeat), there is a corresponding increase in light absorption by the skin. This increase in blood volume leads to greater absorption of light. Consequently, the amount of visible light reflected by the skin changes, forming the basis of photoplethysmography (PPG) signals. Camera-based imaging methods leverage these changes in light absorption to measure variations in blood volume on the skin surface. By analyzing the color and motion changes in the captured video, it becomes possible to extract pulse signals and calculate heart rate frequency.

The ubiquitous camera serves as a *contactless* tool to monitor physiological parameters *at any location and any time*. This is beneficial for three reasons: *i)* Compared to hospital, contact-based sensing methods such as electrocardiography (ECG) and pulse oximetry, ubiquitous camera-based sensing eliminates direct body contact, reducing discomfort and infection risks. *ii)* ubiquitous camera-based sensing seamlessly integrates into environments, enabling *continuous sensing*. Users can be monitored in their *natural settings*, leading to potentially more **accurate and holistic data collection**, compared to limited snapshot measurements in clinical settings. *iii)* Commercial smart devices such as smartphones, laptops, and robots are widely equipped with cameras, making this contactless monitoring method highly accessible and scalable across a wide range of user populations and application scenarios. We identify two application scenarios. Deception detection, such as in criminal suspect lie detection¹, where contactless camera-based heart rate sensors test truthfulness *without the subject's awareness or psychological resistance* [10, 20]. Another application is health monitoring, providing elderly people living independently with a convenient method to monitor their physical data and health status daily.

3 SYSTEM DESIGN

This section begins with an overview of UbiHR before elaborating on its design details.

¹Heart rate-based deception detection deployment requires local authorization.

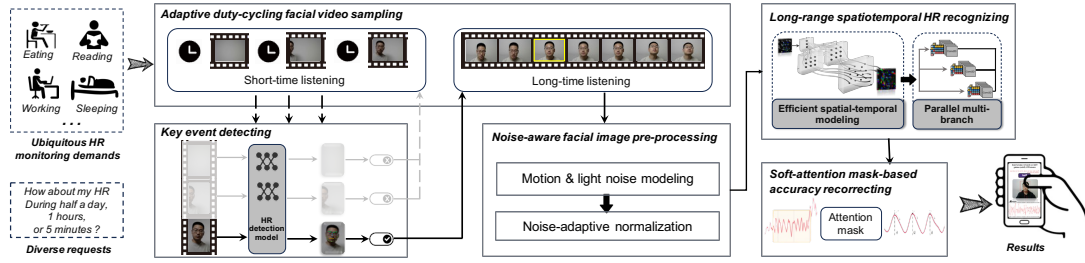


Fig. 4. Workflow of UbiHR system.

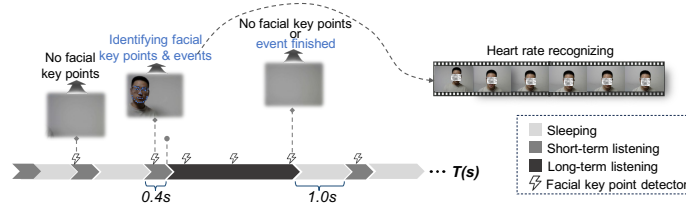


Fig. 5. Illustration of the adaptive duty cycling facial video sensing mechanism (the mosaic is to protect privacy).

3.1 Overview

Figure 4 shows the workflow of UbiHR, which consists of four functional modules, *i.e.*, an *adaptive duty-cycling facial video sampling* module, a *noise-aware facial image preprocessing* module, and a *fast long-range spatiotemporal heart rate recognizing* module. The **adaptive duty-cycling facial video sampling** module switches between sleeping, short-term listening, and long-term listening schemes. It adopts an event-driven adaptive duty-cycling mechanism to balance the energy consumption and the promptness of facial keypoint detection. The **dynamic noise-aware facial image preprocessing** module extracts essential facial key points through differentiation and normalization, eliminating noise from user head motion and varying environmental lighting conditions, and reducing input volume for subsequent processing with real-time performance. The **fast long-range spatiotemporal heart rate recognizing** module incorporates the zero-parameter time shift strategy to 2D convolution for lightweight spatio-temporal modeling, extracting both long-range and short-range spatio-temporal features from the heart rate signal via parallel multi-branch structures, and corrects accuracy using soft-attention masks.

3.2 Adaptive Duty-cycling Facial Video Sampling

This module balances energy cost with efficiency of facial keypoint detection. Continuously operating the camera on battery-powered devices like robots and smartphones consumes significant energy, which is impractical [47, 48]. Given that major heart rate events like sinus bradycardia and high-degree atrioventricular block are rare and brief, UbiHR uses an adaptive duty-cycling mechanism to minimize camera runtime and energy use. It operates in three camera states: *short-term sampling* to detect complete facial images and significant heart rate events, *sleeping* to save energy, and *long-term sampling* for continuous video collection when events are detected.

Figure 5 illustrates an *event-driven, adaptive* duty-cycling mechanism. Initially, the camera starts in *short-term sampling* mode, adjusting for user motion in open environments. An event detector identifies valid video frames and heart rate-related events, shifting to long-term sampling if needed. Studies like [35] and [56] show that the forehead and cheek regions yield the strongest rPPG signals. Only clear, complete facial views are processed further, utilizing an efficient active shape model (ASM)[16] for facial keypoint detection. This model controls shape distribution and predicts motion direction and position of keypoints. If a complete face isn't detected within

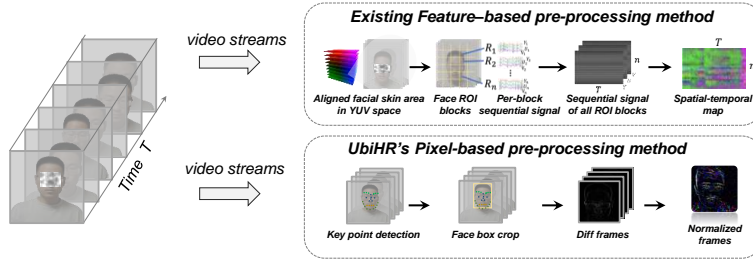


Fig. 6. Comparison of UbiHR and existing pre-processing methods.

0.4s—equivalent to 10 video frames necessary for accurate rPPG detection—the system enters *sleep* mode for 1s. Upon detecting complete faces in short-term mode, we analyze time-domain features of the rPPG signal, such as the pNN50 HRV index[2, 21], to identify critical events like *sinus bradycardia* and *high-degree atrioventricular block*. Specifically, pNN50 measures the percentage of adjacent heartbeats with intervals differing by more than 50ms. A value above 20% indicates high heart rate variability, requiring at least 4 minutes of recording for reliable HRV assessment. In long-term sampling mode, if the pNN50 exceeds 20%, sampling continues until it drops below 20% or the user exits the camera’s view. If pNN50 is under 20%, indicating stability, the camera switches to sleep mode, alternating with short-term sampling for heart rate monitoring. If the average heart rate changes significantly (more than 5×), the system resumes long-term sampling. During critical events, UbiHR enters long-term mode to monitor continuous heart rate fluctuations, processing until 10 consecutive frames lack facial data.

3.3 Dynamic Noise-aware Facial Image Pre-processing

User motion and open environment lighting introduce noise in video frames, necessitating preprocessing for heart rate sensing. Extracting the heart rate directly from raw videos yields a signal contaminated with various interferences. Additionally, the mobility of cameras, such as those on smartphones and robots, complicates matters. Mobile cameras can measure heart rates under any condition but introduce instability and varying angles, causing shaking and lighting changes, which add noise to the heart rate signal. Therefore, preprocessing is crucial to improve the signal-to-noise ratio of the heart rate signal. Prior methods reduce video noises or enhance signal-to-noise ratios for heart rate sensing, mainly include four categories: *i*) Independent Component Analysis (ICA) [63, 64], Principal Component Analysis (PCA)[43], and constrained ICA (cICA)[73] can improve the signal-to-noise ratio of the HR signal from RGB frame sequences. *ii*) Combining HR signals from different Regions of Interest (ROI) using frequency-based weighting [41]. *iii*) Dividing the face into multiple ROI regions to obtain a temporal representation matrix and utilize matrix completion to purify HR-related signals. *iv*) Extracting the feature map from the green channel of frames [32].

However, they struggle to balance accuracy and latency (as we will evaluate in Sec. 4). Mathematical and curve-based methods *i*), *ii*), and *iii*) mathematical and curve-based methods provide quick preprocessing but limited signal-to-noise improvements in heart rate signals. Method *iv*), while promising, is time-consuming, with the STMap approach [58] requiring complex calculations and over 200ms per frame to refine HR signals. To address these challenges, we introduce a novel preprocessing approach that quickly adapts to motion and lighting variations. It employs motion modeling and tailored normalization strategies across consecutive RGB frames, effectively reducing noise from these common real-world variables

In particular, we present a *temporal difference layer*, a dedicated layer designed to compute motion disparities between adjacent frames during pre-processing before input to the deep learning model. Specifically, we employ temporal difference by evaluating brightness changes between adjacent frames, considering factors such as

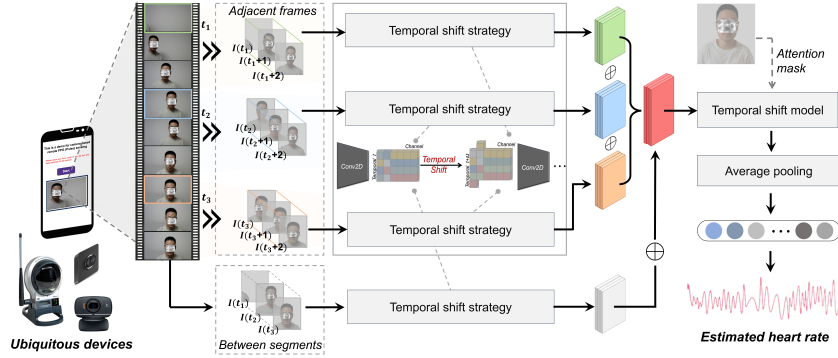


Fig. 7. The architecture of the heart rate recognition model (the mosaic in this paradigm is to protect privacy).

current modulation intensity, specular reflection, diffuse reflection, and optical sensor noise. This differential analysis enables the quantification of differences in diffuse reflection intensity induced by motion. Referencing Equ.(1), which illustrates the optical foundation of differential frames:

$$C_k(t) = (I(t) \cdot (v_s(t) + v_d(t)) + v_n(t)) - (I(t-1) \cdot (v_s(t-1) + v_d(t-1)) + v_n(t-1)) \quad (1)$$

where $C_k(t)$ represents every two consecutive frames and $I(t)$ denotes the modulated luminance intensity influenced by specular reflection $v_s(t)$, diffuse reflection $v_d(t)$, and optical sensor quantization noise $v_s(t)$.

Furthermore, to address the challenge of significant variations in signal scale across frames, especially when the heart rate signal of interest is obscured by subtle pixel variations along the temporal axis, and noise artifacts can result in significantly larger relative changes., we introduce a *learnable batch normalization* layer [51] after the temporal difference layer. This normalization layer incorporates *two learnable parameters*, β and γ , scaling to different variances and shifting to dynamic signal means. This normalization layer ensures that the difference frames within a batch are normalized to the same scale. Equ.(2) demonstrates how the batch normalization layer learns optimal parameters that amplify pixel changes while simultaneously minimizing the impact of noise.

$$N_k(t) = \frac{(\beta_t * D_k(t) + \gamma_t) - \mu D_k}{\sigma D_k} \quad (2)$$

Where μ is mean and σ is standard deviation. Without this normalization step, the frame differences tend to be close to zero, given that subtle variations in user facial skin pixel values between consecutive frames are relatively small. Consequently, batch normalization not only amplifies numerical differences but also normalizes them. Figure 6 compares the contrasting pre-processing workflows of existing methods and ours.

3.4 Fast Long-range Spatio-temporal Heart Rate Recognizing

3.4.1 Primer on Long-range Spatio-temporal Model for HR Detection. Camera-based heart rate recognition involves mapping video sequences to signal sequences. Specifically, it translates the spatial dimension of light reflection in video frames into temporal variations of heart rate signals. As depicted in Figure 8, peak positions exhibit similar characteristics regardless of diverse user heart rate speed or amplitude. Our key observation is that these characteristics include abrupt changes in signal trends and relatively high signal intensity. Therefore, constructing a long-range spatio-temporal model can enhance detection accuracy and robustness.

- **Limitations of Short-range Methods.** Most prior methods extract spatio-temporal rPPG features from *short ranges* [7, 70, 82], such as adjacent frames, overlooking long-range relationships among periodic rPPG features, thereby compromising stability against noise. As illustrated in Tab. 1, compared to scenarios

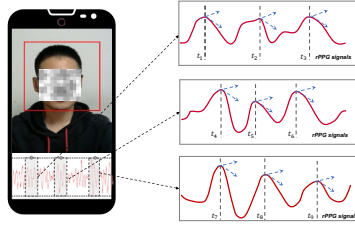


Fig. 8. The user’s heart rate wave varies, while the abrupt transitions at the peak rPPG signal are consistent.

Table 1. Error of two existing short-range methods with different noises.

Short-range Methods	MAE	
	Task1 (Slight head motion)	Task2 (Noisy, user is speaking)
PhysNet [83]	1.86	8.20
DeepPhys [11]	2.11	12.82

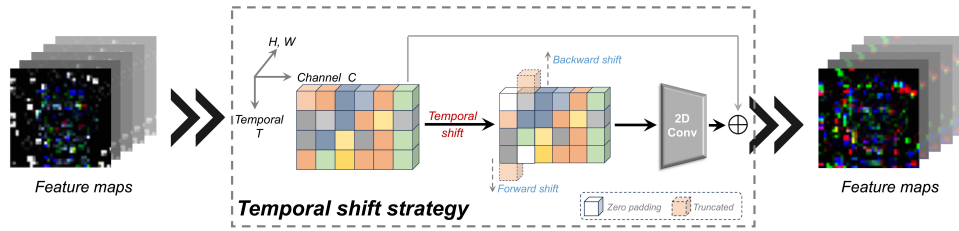


Fig. 9. Illustration of incorporating temporal shift to 2D convolution.

with slight head movements (Task 1), both PhysNet [83] and DeepPhys [11] experience significant Mean Absolute Error (MAE) increases of 6.34 and 10.71, respectively, in high-noise scenarios, such as when the user is speaking (Task 2). Additionally, as mentioned in Sec. 2.3, in practical applications, users often require long-range spatio-temporal awareness of heart rates.

- **Limitations of Long-range Physformer.** A typical long-range spatio-temporal model, *i.e.*, Physformer [84], introduced a transformer architecture that yielded promising accuracy. However, it has 7.03M parameters and 47.01GFLOPs, cannot fit into resource-limited mobile and embedded devices.

To address these, UbiHR need: *i)* operate in real-time to learn noise-robust representations corresponding to pulse and respiration signals from long-range spatio-temporal features, *ii)* be low-cost on resource-constrained mobile and embedded devices, Specifically, even with improved signal-to-noise ratio through preprocessing (see Sec. 3.3), performing rPPG-based heart rate measurement remains challenging due to the subtle amplitude of light absorption variation *inherent* in heart rate signal itself [54]. For example, color distortion, pseudo-color, or color noise caused by camera signal processing algorithms. Also, rPPG signals are sensitive to interference from head motion, lighting conditions, and sensor noises, complicating the construction of a robust tool in less-constrained ubiquitous environments. Therefore, we present a parallel multi-branch model to extract spatio-temporal features across both short and long ranges (Sec. 3.4.3), with a lightweight spatio-temporal model (Sec. 3.4.2).

3.4.2 Incorporating Temporal Shift to 2D Convolution for Lightweight Spatio-temporal Modeling. We utilize a temporal shift strategy to enhance the temporal modeling of 2D convolutions, offering noise-robustness and awareness similar to 3D convolutions, but without the extra computational burden. *3D convolutions* [83] intuitively

enhance the model's robustness and awareness by capturing spatial and temporal variations in frame sequences, effectively mapping heart rate signals. These convolutions progressively extract finer features through multiple layers, differentiating small heart-rate-related signals from larger noise. Additionally, we chose convolutional models over RNN or LSTM because they allow for parallel processing, share kernels across dimensions to reduce parameters and avoid the gradient issues common in sequence processing. Yet, the computational demands of 3D convolutions challenge real-time performance on limited-resource devices.

Therefore, we integrate the zero-parameter temporal shift strategy into 2D Convolution. The temporal shift strategy depicted in Figure 9 enhances temporal modeling efficiency by shifting feature maps along the temporal dimension. It partitions the input tensor into three blocks along the channel dimension, shifting the first block leftward (advancing time by one frame) and the second block rightward (delaying time by one frame). These shifts enrich spatial convolution with temporal feature variations. Notably, tensor shifting introduces no additional parameters to the DL model but facilitates information exchange between adjacent frames. As we will show in Sec. 4, the lightweight spatio-temporal model costs 49% in memory and 3% in latency lower for a 30 frames input.

3.4.3 Multi-branch for Long- and Short-range Spatio-temporal Modeling. Despite its utility, the temporal shift strategy remains confined to short-range spatio-temporal information, limiting its effectiveness in capturing long-range periodic variations in light reflection from sequential video frames. This limitation blocks the model's ability to effectively map long-range heart rate signals. As mentioned in Sec. 3.4.1, capturing the heart rate signal's periodic characteristics over the long-range is pivotal for suppressing non-physiological information like noise, thus enhancing detection accuracy and robustness.

To overcome this challenge, we introduce a multi-branch parallel spatio-temporal model capable of both short- and long-range spatio-temporal modeling. As illustrated in Fig. 7, we partition the input frame sequence into three groups and apply a single-branch temporal shift+2D convolution operation on three adjacent frames, *i.e.*, short-range, within each group. These *short-range branches* function in parallel, combining their results to yield short-range outcomes similar to prior approaches, referred to as the "*adjacent frames branch*". Concurrently, we select one frame from each group in the *adjacent frames branch* to generate a new frame sequence. We conduct a single-branch temporal+2D CNN convolution operation independently on this sequence, creating the "*segment branch*." Operating between frames with longer temporal distances, the segment branch facilitates long-range spatio-temporal modeling. Finally, we merge the outputs of the *adjacent frame branch* (for short range) and the *segment branch* (for long range), performing convolution operations to capture heart rate features consistent across both branches. Accurate mixed-granularity results are then obtained after average pooling.

3.4.4 Towards Parallel Speedup. The multi-branch parallel spatio-temporal model enhances computational efficiency by enabling concurrent convolution operations in the adjacent frames branch, eliminating the sequential processing bottleneck. This parallel execution ensures that subsequent frames can be processed independently of each other, significantly reducing waiting time. Additionally, implementing asynchronous processing further enhances parallelism, reducing waiting time. By grouping consecutive video frames into groups, we exploit parallel capabilities more effectively, accelerating the overall process.

3.4.5 Soft-attention Mask-based Accuracy Recorrecting. Incorporating the temporal shift strategy introduces additional temporal information, potentially leading to noise interference in the processed frames in reverse [50]. This is because temporal shift integrates all the content it moves into the adjacent frames and replaces the original information in those frames, including noise. This can result in the replacement of high-intensity parts of the heart rate signal with noise information or the introduction of heart rate signal information in regions where noise should exist in the current frame. Therefore, it is crucial to prioritize pixels that already contain heart rate information over those affected by temporal shift-induced noises.

To mitigate this, we propose the integration of *soft-attention masks* after each branch and before average pooling. These masks prioritize pixels with existing heart rate information over those affected by temporal shift-induced noise, allowing the network to focus on target signals. Soft-attention masks prioritize pixels that display stronger signals in intermediate convolution representations by assigning them higher weights, reducing the impact of noise. Generated through 1×1 convolutions with pre-processed frames as input, these masks are computed using the sigmoid activation function. Element-wise multiplication is performed with the respective representations from the merge outputs of the adjacent frames branch and segment branch. This strategy ensures that the network effectively discerns and prioritizes pixels with meaningful HR information while attenuating noise interference from the temporal shift. The computation of the attention mask is shown in Equ.(3):

$$\frac{H_j W_j \cdot \sigma(\omega^j \mathbb{X}_\alpha^j + b^j)}{2 \|\sigma(\omega^j \mathbb{X}_\alpha^j + b^j)\|_1} \quad (3)$$

where j is the index of the convolution layer, ω^j is a 1×1 convolution following the sigmoid activation function $\sigma(\cdot)$. And \mathbb{X}_α^j is the feature maps in the convolution layer, H_j and W_j is the height and width. b_j is the bias. Finally, we perform element-wise multiplication with the respective representation from merge outputs of adjacent frames branch and segment branch. As a separate note, if detection remains incorrect, we re-inference erroneous frames and using a longer sequence of video frames to refine the results.

4 EVALUATION

This section presents the experimental settings and system performance of UbiHR.

4.1 Implementation

We train the DL model on the server while conducting heart rate video sampling, detection, and recognition under various motion and lighting conditions on mobile and embedded devices. On the *server side*, UbiHR is implemented in PyTorch (v1.12.1) and utilizes the Adadelta optimizer with a learning rate of 1.0, a batch size of 32, and a 3×3 kernel size with 2×2 pooling. We apply dropout rates of 0.25 and 0.5. All spatio-temporal models use a window size of 10 frames for fair comparison. Model training is accelerated using Nvidia TITAN RTX with CUDA 10.2. On the *client side*, we package the system as a Python module for seamless integration with other applications. Video sampling is performed at 30fps. We integrate existing methods into platforms like Android, primarily overcoming the limited availability of DL-based face recognition libraries. The user interface comprises a viewfinder and a heart rate result display. We design platform-specific user interfaces for various mobile and embedded platforms. The camera viewfinder shows the live feed captured by the camera, with a red box indicating the actual framing area in the center. To protect user privacy, all video frames captured during the duty-cycling sampling process are immediately processed and deleted locally, not sent to the cloud for preprocessing or retained for future processing. Results are displayed as waves using JavaScript, and hovering over the results reveals specific information about corresponding points.

4.2 Experiment setups

Dataset and tasks. We experiment with four datasets. First, both UBFC-RPPG [4] and UBFC-Phys [65] are recorded by low-end cameras instead of professional high-end cameras, under varying sunlight and indoor illumination. UBFC-RPPG features stationary subjects, while UBFC-Phys includes diverse head movements, introducing motion noise. We train on UBFC-RPPG and test on UBFC-Phys to evaluate system performance under diverse motion and lighting noises. Second, we conduct tests on two synthetic datasets, SCAMPS [55] and UCLA-rPPG [77]. SCAMPS synthesized 2800 RGB videos and provided corresponding ground truth PPG signals. It also randomly rendered hair, clothing, and the environment to simulate various real-world scenarios.

UCLA-rPPG synthesized 480 videos based on real videos and PPG signals. It rendered different actions, skin tones, and lighting conditions. Specifically, We first train a backbone with four convolutional layers followed by a tanh activation function for input sequence using UBFC-rPPG. It is captured from a low-end camera (Logitech C920 HD Pro) operating at 30fps and a resolution of 640x480 in uncompressed 8-bit RGB format. Ground truth PPG data, including waveform and heart rates, was acquired using a CMS50E transmissive pulse oximeter. Subjects were positioned approximately 1 meter from the camera, facing it directly. We then employ UBFC-Phys to test system performance. UBFC-Phys are collected from 56 participants undergoing a three-step stress-inducing experience, *e.g.*, a relaxation task (T1), a speech task (T2), and an arithmetic task (T3), to dynamically affect the heart rates.

Ubiquitous devices. We test UbiHR with four commercial mobile camera-embedded platforms, including: *i*) Device D_1 : Raspberry Pi 4B, equipped with a 4-core 1.5GHz ARM Cortex-A72 CPU, is a low-power, single-board computer that is widely used in various embedded and edge computing applications; *ii*) Device D_2 : Nvidia Jetson Orin, equipped with a 4-core ARM Cortex-A78AE CPU, offers significantly higher compute performance compared to the Raspberry Pi, with up to 57 TOPS of AI inference capacity; *iii*) Device D_3 : Nvidia Jetson AGX, equipped with an 8-core ARM Cortex-A78AE CPU, is a high-performance AI computing device designed for advanced robotic, autonomous systems, and edge AI applications and *iv*) Device D_4 : IQOO9 smartphone with the Snapdragon 8Gen1 8-core CPU. With any embedded device equipped with a camera, UbiHR can transform it into a 'heart rate sensing expert assistant,' offering health services in users' daily lives at home.

Baselines. We compare the performance of UbiHR with the following camera-based HR detection baselines.

- **Mathematical/shallow machine learning-based physiological detection methods:**

- **GREEN** [74]: It utilizes the optical reflection of green spectrum on skin blood flow for measurement, which is simple to implement but susceptible to environmental light interference, and is a feature-based method relying on skin optical reflection characteristics.
- **CHROM** [18]: It employs a linear combination of chrominance signals, assuming a standardized skin color profile.
- **POS** [76]: It separates the heart rate information from the optical signal using the principle of pulse occlusion, which can suppress respiration and motion interference, relying on the pulse occlusion model.
- **LGI** [62]: It investigates the influence of prior knowledge regarding invariance on heart rate estimation from face videos captured in real-world conditions.
- **PBV** [19]: It obtains the heart rate information by measuring changes in local skin blood volume, relying on the photoplethysmography blood volume model.
- **ICA** [63]: It separates the heart rate component from multi-channel optical signals, and is relatively robust to motion noises.

- **DL-based HR detection methods:**

- **DeepPhys** [11]: It employs a deep convolutional network for video-based heart and breathing rate sensing.
- **PhysNet** [83]: it uses a deep spatio-temporal network for reconstructing rPPG signals from facial videos.
- **On-device latency-efficient TS-CAN** [50]: It leverages a temporal shift convolutional attention network (TS-CAN) based on hand-crafted pre-processing, to enable HR detection on mobile platforms.
- **On-device latency&memory-efficient UbiHR**: It enables on-device, real-time, and low-memory HR detection through efficient pixel-based preprocessing and a multi-branch parallel spatio-temporal network.

Evaluation metrics. We employ three categories with five metrics to evaluate accuracy as heart rate signals dynamically change over time. *First*, we assess *absolute differences* between predicted and true values using *Mean Absolute Error* (MAE) and *Mean Absolute Percentage Error* (MAPE). While MAE measures absolute differences, MAPE offers a percentage-based explanation, making error interpretation more intuitive. *Second*, we examine the

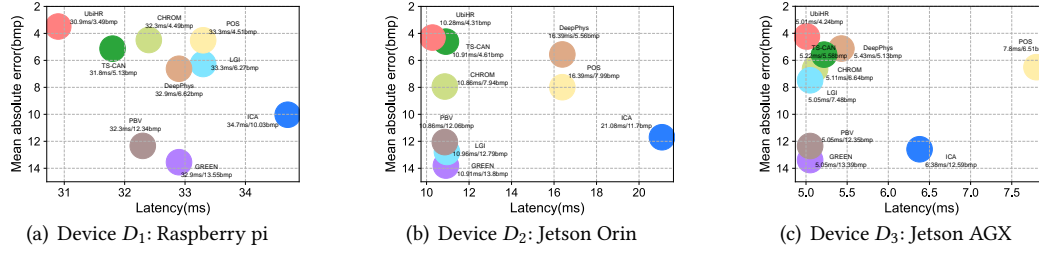


Fig. 10. Trade-off comparison of eight baselines and UbiHR. UbiHR achieves the best overall performance.

relative relationship and *continuity* of continuous HR signals using *root mean square error (RMSE)* and *Pearson coefficient* to capture relative changes and temporal relationships. RMSE, akin to the L2 norm, is sensitive to outliers, unlike MAE, which represents the L1 norm. *Third*, we evaluate *pulse signal-to-noise ratios (SNR)* to gauge system noise robustness. Ground truth HR frequency is obtained from contact pulse oximeters. *Also*, we test UbiHR’s latency and memory usage in real-world mobile and embedded systems.

4.3 Performance comparison

This section presents the results of heart rate sensing compared with the baselines.

4.3.1 Overall trade-off comparison. This experiment compares the performance of UbiHR and nine different baseline methods on open video-based heart rate sensing datasets.

Setups. We conduct tests on three typical mobile and embedded devices, *i.e.*, Device D_1 Raspberry Pi 4B, Device D_2 Nvidia Jetson Orin, and Device D_3 Nvidia Jetson AGX. We use test data of various tasks in UBFC-Phys, *i.e.*, participants performing three tasks under diverse natural lighting conditions: head motion (Task 1), speaking (Task 2), and diverse facial expressions (Task 3), to compare the accuracy, latency, and trade-off of eight different baselines and UbiHR. We test three times on each device and calculate the average values. we use the same inputs on each device, however, these three different devices have different CPU, and their resource constraints led to the use of different processing techniques and different third-party libraries on them.

Results. Figure 10 shows the results, indicating that UbiHR outperforms other baselines across all testing devices. *First*, curve-based methods, *e.g.*, GREEN, CHROM, ICA, LGI, PBV and POS, demonstrate decent latency performance, while these manually designed model-based methods exhibit unacceptable sensing errors on diverse noisy data. *Second*, DeepPhys, tailored for server-side deployment, suffers from 59.4% higher latency (only inference without pre-processing as its pre-processing is too complex to run on mobile and embedded devices) and reduced accuracy on resource-limited mobile and embedded devices due to high-cost pre-processing methods. We note that, due to the high-cost pre-processing methods used in DeepPhys being impractical to deploy on mobile and embedded devices, Figure 10 only presents its inference latency without pre-processing. Even TS-CAN, designed for on-device deployment, processes over 10 frames slower per second than UbiHR due to significant pre-processing and inference overhead.

4.3.2 Accuracy comparison. This experiment compares the heart rate sensing accuracy of baselines and UbiHR.

Setups. We conduct evaluations across three tasks (Task 1 to 3) in UBFC-Phys on Device D_1 Raspberry Pi 4B. Testing two standard accuracy metrics, Mean Absolute Error (MAE) and Mean Absolute Percentage Error (MAPE), with five measurements conducted and the average performance reported. The inputs used for testing different methods are the same.

Results. Fig. 11 summarize the results. *First*, UbiHR achieves the highest accuracy, significantly outperforming curve-based POS with a 22.6% reduction in Mean Absolute Error (MAE) and a 1.32% decrease in Mean Absolute

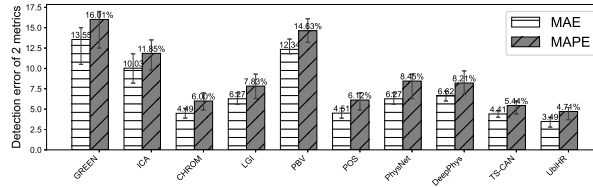


Fig. 11. Detection error comparison of nine baselines and UbiHR.

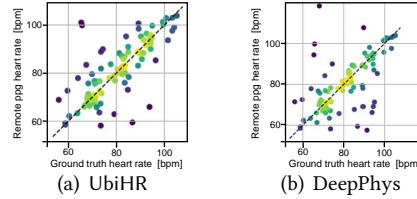


Fig. 12. Comparison of DeepPhys and UbiHR in fitting estimated heart rate to ground truth.

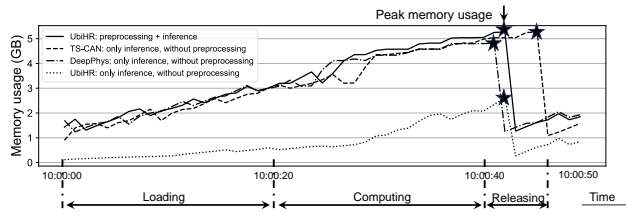


Fig. 13. Memory usage comparison of DeepPhys, TS-CAN, and UbiHR on Raspberry pi 4B.

Percentage Error (MAPE). This superiority is because of the nuanced nature of heart rate variability features, where manually crafted methods like POS may struggle with consistency and are vulnerable to noise. *Second*, compared to existing DL-based methods like TS-CAN, UbiHR reduces MAE by 32% and MAPE by 0.73%, indicating its improved capability to capture intrinsic heart rate features and robustness against noise. *Third*, a Bland-Altman plot (Figure 12) visualizes the correlation between UbiHR’s and DeepPhys’ predicted results and ground truth. Comparing the plots, UbiHR demonstrates a stronger correlation between predicted and actual heart rates, particularly in the 60 bpm to 110 bpm range of the UBFC-Phys dataset, with fewer outlier values.

4.3.3 *Memory usage comparison.* This experiment evaluates the memory usage of UbiHR compared to baselines.

Setups. Using three continuous video clips from UBFC-Phys on Raspberry Pi 4B, with durations of 3 minutes, we monitor the memory usage during the inference process. For other baselines, as the preprocessing steps couldn’t be performed on Raspberry Pi 4B, preprocessed data are used as their input. We use the rPPG-Toolbox for fair testing. The memory usage data of the devices is collected by using the professional tool called dstat.

Results. Figure 13 illustrates the memory usage of TS-CAN and DeepPhys, which are used solely for inference due to the high-cost preprocessing can not fit into embedded devices. While we show the memory usage of both inference and the entire end-to-end process with UbiHR. *First*, UbiHR’s memory usage of inference reveals the lowest memory usage. *Second*, UbiHR’s end-to-end process exhibits an average memory usage of 2.32GB, which is 1.25% higher than TS-CAN and 15.71% higher than DeepPhys. This indicates that UbiHR’s on-device pre-processing and multi-branch spatio-temporal model are low-cost. *Third*, all three methods exhibit periodic memory usage fluctuations during continuous operation, gradually increasing and decreasing at certain intervals. For TS-CAN and DeepPhys, this is due to the need to read pre-processed data in npy format before inference.

Table 2. Inference latency comparison of DL-based baselines and UbiHR on three devices.

Method	Frame number inferred per second (FPS) on different device		
	Raspberry pi	Jetson Orin	Jetson AGX
DeepPhys [11]	27.6	61.1	184.2
TS-CAN [50]	28.6	91.7	191.6
UbiHR	30.1	98.3	201.8

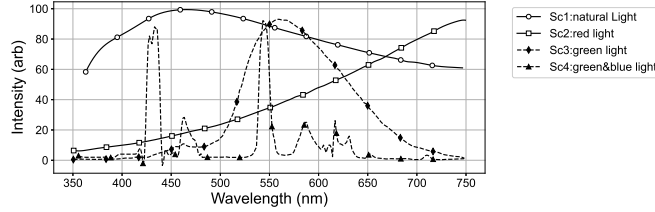


Fig. 14. Spectrum illustration of different light conditions.

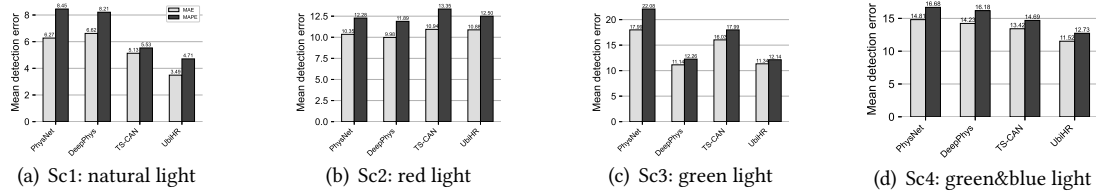


Fig. 15. Accuracy comparison of three DL-based baselines and UbiHR under diverse light conditions.

UbiHR conducts on-device pre-processing and inference, requiring reading frames and storing them in memory until a predefined size is reached, at which the memory is released.

4.3.4 Latency comparison. This experiment compares the latency of UbiHR and different baseline methods.

Setup. The baseline and data setups are consistent with the previous one. We test the latency across three devices: Raspberry Pi 4B, Jetson Orin, and Jetson AGX. We measure the FPS (Frames Per Second) as the metric.

Results. Table 2 shows the results. *First*, UbiHR exhibits the fastest inference speed on all devices. On the Raspberry Pi, it shows a 9.06% improvement over DeepPhys and a 5.24% improvement over TS-CAN. On the Orin and AGX devices, UbiHR achieves speed improvements of 60.88% and 9.55% respectively over DeepPhys and 7.19% and 5.32% over TS-CAN. *Second*, as device performance increases, UbiHR demonstrates the most significant increase in inference speed. From the Raspberry Pi to the AGX, its speed increases by 171.7fps, compared to 156.6fps for DeepPhys and 163fps for TS-CAN. This improvement is attributed to the lightweight and parallel spatio-temporal model structure, reducing computing costs.

4.4 Performance over Diverse Light Conditions

This experiment assesses the sensing stability of UbiHR and three DL-based baseline methods across four real-world scenarios. Varying light conditions introduce different spectra and frequencies, leading to diverse signal-to-noise ratios. User motions further lead to noises, challenging the stability of heart rate sensing performance.

Setups. We adopt four light conditions that users always encounter, *i.e.*, natural light (Sc1), red light (Sc2), green light (Sc3), and mixed blue-green light (Sc4). These scenarios represent various ubiquitous application environments such as natural outdoor lighting, red light resembling incandescent bulbs, green light resembling fluorescent lamps, and a mix of green and blue light resembling LED lights. To simulate these conditions, we applied different spectral filters to videos captured under natural lighting (Sc1) using OpenCV. These videos also feature diverse motions from users.

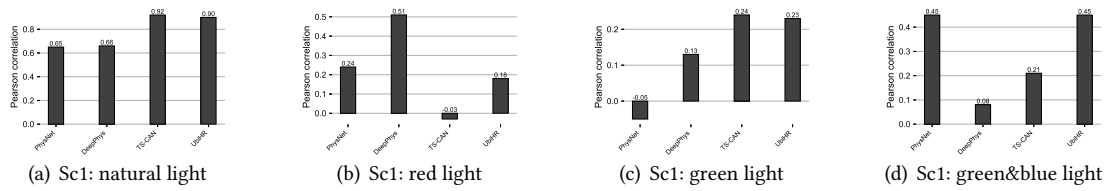


Fig. 16. Pearson correlation comparison of three baselines and UbiHR under diverse light conditions.

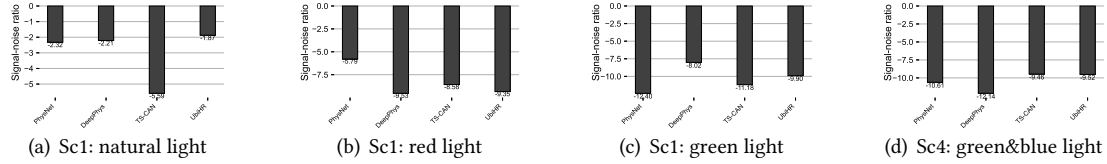


Fig. 17. Signal-noise ratio comparison of three baselines and UbiHR under diverse light conditions.

Results. As shown in Fig. 14, natural light offers a broad spectrum with uniform frequencies, resulting in ideal optical reflection from the skin. In contrast, artificial indoor light sources emit specific frequencies. *First*, in Fig. 15, UbiHR shows the best stability with a minimal MAE fluctuation of 0.64, outperforming DeepPhys (MAE fluctuation: 4.25), which excels under red and green lights but struggles under blue-green. PhysNet and TS-CAN exhibit higher fluctuations (7.74 and 5.09, respectively). UbiHR’s stability is attributed to its long-range multi-branch network, adept at capturing heart rate variations and reducing noise impact even with drastic lighting changes. Also, all methods perform better under red light but face challenges under green due to variations in blood’s light absorption properties, with red light experiencing less interference and green light fluctuations causing more significant optical changes, affecting accuracy. *Second*, in terms of the correlation between predicted and actual heart rate signals, UbiHR demonstrates superior stability. PhysNet and TS-CAN exhibit negative correlations under green and red light conditions, respectively. DeepPhys shows a weak correlation coefficient of only 0.08 under blue-green mixed light, also considered unacceptable. While UbiHR not only shows better correlations across conditions but also maintains relatively small fluctuations, affirming its adeptness at learning intrinsic heart rate signal variations. Third, we assess the signal-to-noise ratio (SNR), indicating a method’s noise resistance, where lower values imply stronger noise resistance, considering the weak BVP signal against strong noise. UbiHR excels in SNR performance under natural light, outpacing TS-CAN by 67.6%. Also, it maintains stability under other lighting conditions, avoiding sudden/significant performance drops.

4.5 Performance with Diverse Input Range

This experiment confirms the effectiveness of UbiHR’s long-range spatio-temporal model compared to baseline methods relying on short-range adjacent frames. As mentioned in Sec. 3.4, previous methods always utilize a single-branch structure, such as TS-CAN [50], restricting their capability to establish mappings from videos to heart rate signals only within short ranges. While UbiHR adopts a multi-branch parallel spatio-temporal model, enabling simultaneous capture of spatio-temporal relationships across short and long ranges.

Setup. We perform experiments on Device D_1 using the same three input video segments as discussed in Sec. 4.3.3. We vary the number of frame sequences inputted to TS-CAN and UbiHR, ranging from adjacent 5 to 30 frames, to investigate the influence of different input quantities on inference accuracy. Each input undergoes 5 times to show the average value.

Results. Fig. 18 illustrates the changes in heart rate prediction error for UbiHR and TS-CAN with increasing input frame ranges. TS-CAN exhibits a gradual increase in error as the input frame range rises, whereas UbiHR

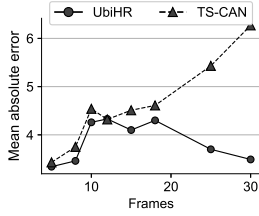


Fig. 18. Impact of input frame number.

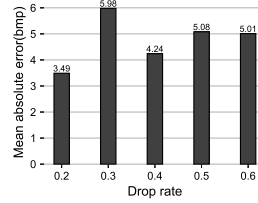


Fig. 19. Impact of drop rates.

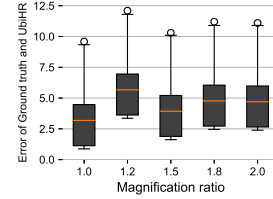


Fig. 20. Impact of face box size.

Table 3. Performance of with/without soft-attention mask in UbiHR.

Error metrics	Ablation set	
	With attention mask	Without attention mask
MAE	3.49	6.81
MAPE	4.65	8.67
RMSE	6.01	13.62
Pearson	0.90	0.45
SNR	-2.21	-4.61

Table 4. Performance on mobile phone iQOO9 of UbiHR.

Device	Latency	Testing error(MAE)		
		UBFC-Phys	SCAMPS	UCLA-rPPG
iQOO 9	12.4ms	4.13	5.07	5.28

maintains a relatively stable error rate between 3.5% and 5%. The difference in error is minimal when the input frame range is around 12 frames for TS-CAN but gradually widens thereafter. Notably, when utilizing a range of 30 frames as input, UbiHR achieves an error reduction of approximately 44% compared to TS-CAN. Therefore, in TS-CAN [50], the default input is limited to 10 frames.

4.6 Performance on Diverse Testing Data

This experiment validates the inference speed and robustness of UbiHR in diverse testing data, on the smartphone (D_4). We deploy the model pre-trained on UBFC-rppg, and test it on three different datasets (UBFC-Phys, SCAMPS, and UCLA-rPPG). To simulate real-world scenarios, we maintain the resource-competing processes on the mobile phone. The results summarized in Tab. 4 indicate that UbiHR achieves an inference speed of 12.4ms per frame on the Snapdragon 8 Gen1 CPU, meeting real-time detection requirements in practical scenarios. Moreover, in terms of inference accuracy, UbiHR achieves MAE values of 4.13, 5.07, and 5.28 on the three different datasets, respectively, demonstrating robustness in real-world application scenarios.

4.7 Micro-benchmark and Ablation studies

4.7.1 Impact of Drop Rate. We examine the influence of various Drop Rates during UbiHR’s model training. As mentioned in Sec. 3.4.2, we utilize 2D convolution kernels and the drop rate is an important parameter that affects its learning effectiveness. As depicted in Fig. 19, the optimal Drop Rate in UbiHR’s training process is 0.2. Further elevating this parameter diminishes both model performance and robustness.

4.7.2 Impact of Face Box Size. We test the influence of the size of the face bounding box formed by key point detection on UbiHR’s accuracy. As depicted in Fig. 20, continuously increasing the enlargement ratio of the face bounding box results in decreased performance and stability of UbiHR. This is because enlarging the face bounding box introduces background noise, thus affecting accuracy.



(a) S_1 : dormitory (b) S_2 : meeting room (c) S_3 : cafe

Fig. 21. Three real-world case studies in real-world scenarios.

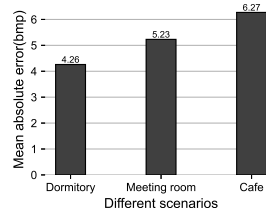


Fig. 22. Performance in different scenarios



Fig. 23. Comparison of ChatGPT’s advice to heart health issues: (a) Generic healthcare prompt; (b) Incorporating UbiHR’s real-time heart rate sensing result into prompt

4.7.3 *Impact of Soft-attention Mask.* As discussed in Sec. 3.4.5, directly integrating the spatio-temporal module to 2D convolution introduces extra spatio-temporal noise, diverting the network’s attention to pixels devoid of physiological signals. Thus, we introduce the soft-attention mask as a correction. Table 3 compares the performance of UbiHR on the UBFC-Phys test data with and without the soft-attention mask. It’s evident that without the soft-attention mask, UbiHR’s accuracy notably declines across all 5 metrics.

4.8 Case study

To investigate the performance of UbiHR in various real-world scenarios, we conduct tests using a smartphone (D_4) across multiple real-world settings. As shown in Fig. 21, we select three scenarios for testing: *i)* Dormitory: features stable fluorescent lighting with minimal background pedestrian traffic, making it close to an ideal experimental environment. *ii)* Meeting room: similar to the dormitory, it has stable lighting from natural light or LED lamps but is larger and more complex, with potential interference from objects and moving people. *iii)* Cafe: the most complex environment, combining natural, fluorescent, and LED lighting, with a physically intricate setting and high pedestrian traffic. We assess UbiHR’s inference accuracy in these progressively complex real-world scenarios. We use the front camera of the smartphone to record a 10-minute video, and then performed heart rate monitoring through the UbiHR system deployed on the smartphone while the user wearing professional heart rate monitoring equipment. The results are shown in the Fig. 22, in different scenarios, the MAE of UbiHR are 4.26, 5.23, and 6.27 respectively. This is consistent with our expectation, that is, the more complex the lighting conditions and the environment, the greater the noise in UbiHR’s inference, and the higher the error rate. Even so, UbiHR still maintains a relatively high accuracy in the most complex scenario.

Large Language Models (LLMs), exemplified by OpenAI’s ChatGPT, have demonstrated success in the healthcare field [68, 81]. However, when addressing cardiovascular diseases, LLMs often provide vague answers due to the lack of accurate and real-time user physiological data. To showcase the application value and performance of UbiHR, we conduct a practical case study using ChatGPT on mobile devices. We compare the outputs of ChatGPT under two scenarios: direct user inquiries for health advice and integration of real-time heart rate sensing results from UbiHR into the query prompt. In Fig. 23a, when a user seeks healthcare advice from ChatGPT without real-time physiological data, the response lacks specificity. In Fig. 23b, with the integration of real-time heart rate data from UbiHR, the specificity and assistance of the response are significantly improved.



Fig. 24. Real-time heart rate of the participants. Fig. 25. Changes in memory usage and power consumption.

We conduct tests to evaluate the system overhead of deploying UbiHR on a smartphone (D_4). Using the front-facing camera, we perform a 55-minute long-duration test to monitor participants' heart rate fluctuations, as illustrated in Fig. 24. In terms of memory usage, we observe an average usage of 660.5MB, with a peak usage of 762MB. The front-facing camera accounts for approximately 532MB, while UbiHR occupies around 230MB. Regarding power consumption, the UbiHR system exhibits an average power consumption of 2.77W, with a peak consumption of 3.3W. The front-facing camera consumes approximately 2.2W, while UbiHR's inference consumes around 1.1W. Thanks to the adaptive duty cycling mechanism, UbiHR reduces memory usage and power consumption by 13.3% and 19% respectively compared to continuous inference. This optimization enables UbiHR to operate with low resource usage and power cost, making it suitable for deployment on various mobile platforms for long-term heart rate sensing.

5 RELATED WORK

Our work is related to the following categories of research.

5.1 Mobile Health Monitoring Powered by Machine Learning

Biometric signal sensors powered by machine learning, focusing on important biosignals: electrocardiogram (ECG), electromyogram (EMG), electroencephalogram (EEG), and photoplethysmogram (PPG) has already achieved widespread research and application. [39]. Furthermore, the diagnostic and monitoring capabilities for diseases such as Inflammatory Bowel disease (IBD) [30] and Breast diseases [1] have also seen tremendous improvements with the help of deep learning models. Apart from the development of deep learning combined with personalized healthcare research [8], this can be attributed to the development of various wearable or non-invasive health monitoring and assistive devices [37]. The widespread adoption and development of cameras have also provided the hardware foundation for researching video-based non-contact heart rate monitoring systems.

5.2 Heart rate sensing tools

Contact-based heart rate sensing tools are widely used for heart rate measurement across various crowds to continuously monitor health conditions [22, 36]. However, prolonged wearing of contact-based monitors such as finger clips or chest straps could cause discomfort for users and may impact their daily lives. Wearable devices, *e.g.*, wristbands [9], eyeglasses [14], and AR/VR headsets [40, 85], are gradually becoming integrated into people's daily lives. For example, EmoTracer [75] integrates a blood oxygen module and a heart rate module into a wristband-type sensor for acquiring physiological signals. Some studies use smartphone cameras [67] or other sensors, *e.g.*, GPS [31], to perform contact-based measurement or estimation. Nevertheless, the positioning of devices on different body locations can also lead to variations in measurement results. Therefore, adopting non-contact methods for heart rate sensing will be more convenient and efficient for users.

5.3 Function-based visual heart rate sensing

To address the limitations of contact-based heart rate sensing, remote heart rate sensing has garnered increasing attention. Among these approaches, remote photoplethysmography (rPPG) has emerged as an important

alternative to existing sensing tools, as it solely relies on a camera [71]. Function-based visual heart rate sensing approaches endeavor to extract heart rate signals from facial videos based on mathematics and designed models, such as independent component analysis (ICA) [79], blind source separation (BSS) [64], and chrominance model [43]. Guo et al. [27] utilize joint BSS to analyze color signal changes from multiple facial sub-regions for remote heart rate sensing. POS [76] incorporates the relevant optical and physiological properties of skin reflections, using a projection plane orthogonal to the skin-tone for pulse extraction. Nevertheless, function-based methods lack robustness when detecting in complex surroundings or under obvious changes in lighting conditions. UbiHR enhances the anti-interference capability against real-world sensing scenario noise through a series of heart rate sampling and preprocessing steps, aiming to provide more accurate heart rate sensing results.

5.4 DL-based heart rate sensing

Constantly evolving deep learning (DL) techniques have laid the foundation for more accurate and robust visual heart rate sensing [17, 70]. Specifically, CNN-based approaches utilize feature extraction networks to obtain high-quality rPPG signals and then estimate heart rates based on signal features, mainly including 2D CNN [11, 50, 57] and 3D CNN [61, 83]. To capture richer temporal information of rPPG, RNN have been incorporated into heart rate sensing to mitigate sensing data noise [5], model the correlation between adjacent frames [58], and extract global temporal information from continuous facial video frames [34]. For example, Lee et al. [42] integrate meta learning with LSTM to enhance the adaptability of heart rate sensing models to random variations in facial videos. Furthermore, GAN have been employed to compute higher-quality ROI for heart rate sensing [54]. PulseGAN [69] derives an initial rPPG signal from the delineated ROI, which is subsequently utilized as input to generate realistic rPPG signals. Additionally, the performance of Transformers [28, 84] has been validated in modeling long-term dependencies of rPPG signals. However, these methods necessitate substantial computational and storage resources during both training and inference, posing challenges for their deployment on resource-constrained smart devices. UbiHR builds upon prior research efforts to develop a lightweight heart rate sensing system capable of operating on ubiquitous devices.

5.5 Resource-efficient on-device heart rate sensing

Deploying advanced AI models on resource-constrained smart devices for continuous heart rate sensing remains a challenging research endeavor [50, 52]. To make sensing models more lightweight, Comas et al. [15] incrementally combining multiple convolutional derivatives to model rPPG dynamics. RtrPPG [6] optimizes inference time through methods such as input size reduction, and RGB to YUB color space transformation. Similarly, Efficientphys [51] strives to minimize the computational overhead and inference time of the entire model by minimizing the need for face segmentation, normalization, color space transformation, or any other unnecessary preprocessing steps. Moreover, Liu et al. [53] combine empirical mode decomposition with channel-wise lightweight CNN to infer heart rate. Some researchers have also utilized the shallow encoder-decoder framework [12] to achieve resource-efficient heart rate sensing. UbiHR follows this research trend of cultivating resource-efficient on-device heart rate sensing systems. It performs real-time heart rate sensing by applying energy-efficient data sampling and concise facial video frame pre-processing techniques.

5.6 Spatio-temporal DL model

Spatio-temporal modeling is an essential part of heart rate sensing, as the rPPG signal reflects both subtle local color changes indicating blood volume variations and periodic changes corresponding to the cardiac cycle. Effective spatio-temporal modeling is necessary to identify relevant facial regions and track rPPG evolution. Spatio-temporal DL models primarily leverage combinations of 2D CNN and RNN [42], two-stage CNN [78], and 3D CNN [83] (or combined with Temporal Shift Models [46, 50]) to accurately capture the rPPG signal. For

instance, CVD [59] transforms facial videos into multi-scale spatio-temporal maps, preserving the temporal characteristics of periodic physiological signals while suppressing redundant data. Yu et al. [82] utilize Temporal Difference Convolution (TDC) to capture intrinsic rPPG-aware clues between facial video frames and then use spatio-temporal data augmentation strategies for rPPG extraction. To reduce redundant spatial information, SAM [33] transforms long-range spatio-temporal feature maps into short-segment spatio-temporal feature maps, followed by spatio-temporal strip pooling and attention mechanisms to extract rPPG signals. However, since the rPPG signal may span multiple cardiac cycles, long-range spatio-temporal modeling can better capture the long-term dependencies and periodicity in the rPPG signal compared to short-range spatio-temporal modeling, effectively handling heart rate variations and irregular rhythms. To this end, UbiHR designs a simple yet effective preprocessing method based on image differencing, along with a long-range spatio-temporal modeling network, enhancing the robustness of measurements in different environments while ensuring minimal latency.

6 CONCLUSION

This paper presents UbiHR, a real-time on-device heart rate sensing system on resource-constrained ubiquitous devices. UbiHR is the first work that realizes end-to-end real-time noise-robust long-range spatio-temporal heart rate sampling, pre-processing, and recognizing. It includes adaptive duty-cycling facial video sampling, dynamic noise-aware facial image pre-processing, and fast long-range spatio-temporal heart rate recognition. Evaluations on 4 datasets and real-world scenarios over four mobile and embedded devices show that UbiHR achieves latency reductions of up to 51.2%, and accuracy improvements of up to 74.2%. In the future, we plan to integrate UbiHR with the large language model-based interaction robotics, creating the real-time on-device physiological sensing and interaction system loop.

REFERENCES

- [1] João Abrantes, Maria João Silva, José Meneses, Catarina Oliveira, Francisco Maria Calisto, and Ross Filice. 2023. External validation of a deep learning model for breast density classification. *ESR—European Society of Radiology: Vienna, Austria* (2023).
- [2] Solange Akselrod, David Gordon, F Andrew Ubel, Daniel C Shannon, A Clifford Berger, and Richard J Cohen. 1981. Power spectrum analysis of heart rate fluctuation: a quantitative probe of beat-to-beat cardiovascular control. *science* 213, 4504 (1981), 220–222.
- [3] Leonardo Alchieri, Nouran Abdalazim, Lidia Alecci, Shkurta Gashi, Elena Di Lascio, and Silvia Santini. 2022. On the Impact of Lateralization in Physiological Signals from Wearable Sensors. In *Adjunct Proceedings of the 2022 ACM International Joint Conference on Pervasive and Ubiquitous Computing and the 2022 ACM International Symposium on Wearable Computers*. 472–477.
- [4] Serge Bobbia, Richard Macwan, Yannick Benezeth, Alamin Mansouri, and Julien Dubois. 2019. Unsupervised skin tissue segmentation for remote photoplethysmography. *Pattern Recognition Letters* 124 (2019), 82–90.
- [5] Deivid Botina-Monsalve, Yannick Benezeth, Richard Macwan, Paul Pierrart, Federico Parra, Keisuke Nakamura, Randy Gomez, and Johel Miteran. 2020. Long short-term memory deep-filter in remote photoplethysmography. In *Proceedings of the IEEE/CVF Conference on Computer Vision and Pattern Recognition Workshops*. 306–307.
- [6] Deivid Botina-Monsalve, Yannick Benezeth, and Johel Miteran. 2022. RT-rPPG: An ultra light 3DCNN for real-time remote photoplethysmography. In *Proceedings of the IEEE/CVF Conference on Computer Vision and Pattern Recognition*. 2146–2154.
- [7] Frédéric Bousefsaf, Alain Pruski, and Choubeila Maaoui. 2019. 3D convolutional neural networks for remote pulse rate measurement and mapping from facial video. *Applied Sciences* 9, 20 (2019), 4364.
- [8] Francisco Maria Calisto, Nuno Nunes, and Jacinto C Nascimento. 2022. Modeling adoption of intelligent agents in medical imaging. *International Journal of Human-Computer Studies* 168 (2022), 102922.
- [9] Yetong Cao, Fan Li, Huijie Chen, Xiaochen Liu, Li Zhang, and Yu Wang. 2022. Guard Your Heart Silently: Continuous Electrocardiogram Waveform Monitoring with Wrist-Worn Motion Sensor. *Proceedings of the ACM on Interactive, Mobile, Wearable and Ubiquitous Technologies* 6, 3 (2022), 1–29.
- [10] Hung-Chang Chang. 2023. Noncontact Lie detection system involving photoplethysmography and heart rate variability. *International Journal of Pattern Recognition and Artificial Intelligence* 37, 07 (2023), 2350006.
- [11] Weixuan Chen and Daniel McDuff. 2018. Deepphys: Video-based physiological measurement using convolutional attention networks. In *Proceedings of the european conference on computer vision (ECCV)*. 349–365.
- [12] Moajjem Hossain Chowdhury, Muhammad EH Chowdhury, Mamun Bin Ibne Reaz, Sawal Hamid Md Ali, Seyed Mehdi Rakhtala, M Murugappan, Sakib Mahmud, Nazmul Islam Shuzan, Ahmad Ashrif A Bakar, Mohd Ibrahim Bin Shapiai, et al. 2024. LGI-rPPG-Net: A

- shallow encoder-decoder model for rPPG signal estimation from facial video streams. *Biomedical Signal Processing and Control* 89 (2024), 105687.
- [13] Patrick Chwalek, David Ramsay, and Joseph A Paradiso. 2021. Captivates: A smart eyeglass platform for across-context physiological measurement. *Proceedings of the ACM on Interactive, Mobile, Wearable and Ubiquitous Technologies* 5, 3 (2021), 1–32.
- [14] Patrick Chwalek, David Ramsay, and Joseph A Paradiso. 2023. Captivates: A Smart Eyeglass Platform for Across-Context Physiological Measurements. *GetMobile: Mobile Computing and Communications* 27, 2 (2023), 18–22.
- [15] Joaquim Comas, Adria Ruiz, and Federico Sukno. 2022. Efficient remote photoplethysmography with temporal derivative modules and time-shift invariant loss. In *Proceedings of the IEEE/CVF Conference on Computer Vision and Pattern Recognition*. 2182–2191.
- [16] Timothy F Cootes, Christopher J Taylor, David H Cooper, and Jim Graham. 1995. Active shape models-their training and application. *Computer vision and image understanding* 61, 1 (1995), 38–59.
- [17] Emil Dark, Umer Saleem, Arttu Lämsä, Constantino Álvarez Casado, and Miguel Bordallo López. 2022. Heart Rate Estimation from Noisy PPGs Using 1D/2D Conversion and Transfer Learning. In *Adjunct Proceedings of the 2022 ACM International Joint Conference on Pervasive and Ubiquitous Computing and the 2022 ACM International Symposium on Wearable Computers*. 163–167.
- [18] Gerard De Haan and Vincent Jeanne. 2013. Robust pulse rate from chrominance-based rPPG. *IEEE transactions on biomedical engineering* 60, 10 (2013), 2878–2886.
- [19] Gerard De Haan and Arno Van Leest. 2014. Improved motion robustness of remote-PPG by using the blood volume pulse signature. *Physiological measurement* 35, 9 (2014), 1913.
- [20] Geoffrey Duran, Isabelle Tapiero, and George A Michael. 2018. Resting heart rate: A physiological predictor of lie detection ability. *Physiology & behavior* 186 (2018), 10–15.
- [21] Task Force of the European Society of Cardiology the North American Society of Pacing Electrophysiology. 1996. Heart rate variability: standards of measurement, physiological interpretation, and clinical use. *Circulation* 93, 5 (1996), 1043–1065.
- [22] Illia Fedorin, Kostyantyn Slyusarenko, Vitalii Pohribnyi, JongSeok Yoon, Gunguk Park, and Hyunsu Kim. 2021. Heart rate trend forecasting during high-intensity interval training using consumer wearable devices. In *Proceedings of the 27th Annual International Conference on Mobile Computing and Networking*. 855–857.
- [23] Kim Fox, Jeffrey S Borer, A John Camm, Nicolas Danchin, Roberto Ferrari, Jose L Lopez Sendon, Philippe Gabriel Steg, Jean-Claude Tardif, Luigi Tavazzi, Michal Tendera, et al. 2007. Resting heart rate in cardiovascular disease. *Journal of the American College of Cardiology* 50, 9 (2007), 823–830.
- [24] Alessandra Frattola, Gianfranco Parati, Cesare Cuspidi, Fabio Albinì, and Giuseppe Mancina. 1993. Prognostic value of 24-hour blood pressure variability. *Journal of hypertension* 11, 10 (1993), 1133–1137.
- [25] Benjamin S Geisler, Frank Brandhoff, Jens Fiehler, Christian Saager, Oliver Speck, Joachim Rother, Hermann Zeumer, and Thomas Kucinski. 2006. Blood oxygen level-dependent MRI allows metabolic description of tissue at risk in acute stroke patients. *Stroke* 37, 7 (2006), 1778–1784.
- [26] Amogh Gudi, Marian Bittner, Roelof Lochmans, and Jan Van Gemert. 2019. Efficient real-time camera based estimation of heart rate and its variability. In *Proceedings of the IEEE/CVF International Conference on Computer Vision Workshops*. 0–0.
- [27] Zhenyu Guo, Z Jane Wang, and Zhiqi Shen. 2014. Physiological parameter monitoring of drivers based on video data and independent vector analysis. In *2014 IEEE International Conference on Acoustics, Speech and Signal Processing (ICASSP)*. IEEE, 4374–4378.
- [28] Anup Kumar Gupta, Rupesh Kumar, Lokendra Birla, and Puneet Gupta. 2023. Radiant: Better rppg estimation using signal embeddings and transformer. In *Proceedings of the IEEE/CVF Winter Conference on Applications of Computer Vision*. 4976–4986.
- [29] MMA Hashem, Rushdi Shams, Md Abdul Kader, and Md Abu Sayed. 2010. Design and development of a heart rate measuring device using fingertip. In *International Conference on Computer and Communication Engineering (ICCCCE'10)*. IEEE, 1–5.
- [30] Robert P Hirtten, Kai-Chun Lin, Jessica Whang, Sarah Shahub, Nathan KM Churcher, Drew Helmus, Sriram Muthukumar, Bruce Sands, and Shalini Prasad. 2024. Longitudinal monitoring of IL-6 and CRP in inflammatory bowel disease using IBD-AWARE. *Biosensors and Bioelectronics: X* 16 (2024), 100435.
- [31] Nutta Homdee, Mehdi Boukhechba, Yixue W Feng, Natalie Kramer, John Lach, and Laura E Barnes. 2019. Enabling Smartphone-based Estimation of Heart Rate. *arXiv preprint arXiv:1912.08910* (2019).
- [32] Gee-Sern Hsu, ArulMurugan Ambikapathi, and Ming-Shiang Chen. 2017. Deep learning with time-frequency representation for pulse estimation from facial videos. In *2017 IEEE international joint conference on biometrics (IJCB)*. IEEE, 383–389.
- [33] Min Hu, Fei Qian, Xiaohua Wang, Lei He, Dong Guo, and Fuji Ren. 2021. Robust heart rate estimation with spatial-temporal attention network from facial videos. *IEEE Transactions on Cognitive and Developmental Systems* 14, 2 (2021), 639–647.
- [34] Bin Huang, Chun-Liang Lin, Weihai Chen, Chia-Feng Juang, and Xingming Wu. 2021. A novel one-stage framework for visual pulse rate estimation using deep neural networks. *Biomedical Signal Processing and Control* 66 (2021), 102387.
- [35] Ramin Irani, Kamal Nasrollahi, and Thomas B Moeslund. 2014. Improved pulse detection from head motions using DCT. In *2014 international conference on computer vision theory and applications (VISAPP)*, Vol. 3. IEEE, 118–124.
- [36] Yusuke Kawasaki, Tahera Hossain, Anna Yokokubo, and Guillaume Lopez. 2021. Estimating the Degree of Mental State using Heart Rate while Studying. In *Adjunct Proceedings of the 2021 ACM International Joint Conference on Pervasive and Ubiquitous Computing and*

- Proceedings of the 2021 ACM International Symposium on Wearable Computers*. 126–130.
- [37] Nikolay L Kazanskiy, Svetlana N Khonina, and Muhammad A Butt. 2024. A review on flexible wearables-Recent developments in non-invasive continuous health monitoring. *Sensors and Actuators A: Physical* (2024), 114993.
- [38] Bartłomiej Kiczek, Dariusz Wójcik, Michał Oleszek, Tomasz Rymarczyk, Jan Sikora, Bartłomiej Baran, and Bartosz Przysucha. 2022. LETS-a Wearable Heart and Lung Monitoring Device for the Diagnosis of Cardiac and Respiratory Diseases. In *Adjunct Proceedings of the 2022 ACM International Joint Conference on Pervasive and Ubiquitous Computing and the 2022 ACM International Symposium on Wearable Computers*. 60–62.
- [39] Dohyung Kim, JinKi Min, and Seung Hwan Ko. 2024. Recent developments and future directions of wearable skin biosignal sensors. *Advanced Sensor Research* 3, 2 (2024), 2300118.
- [40] Gwangbin Kim, Jieun Lee, Dohyeon Yeo, Eunsol An, and SeungJun Kim. 2023. Physiological Indices to Predict Driver Situation Awareness in VR. In *Adjunct Proceedings of the 2023 ACM International Joint Conference on Pervasive and Ubiquitous Computing & the 2023 ACM International Symposium on Wearable Computing*. 40–45.
- [41] Mayank Kumar, Ashok Veeraraghavan, and Ashutosh Sabharwal. 2015. DistancePPG: Robust non-contact vital signs monitoring using a camera. *Biomedical optics express* 6, 5 (2015), 1565–1588.
- [42] Eugene Lee, Evan Chen, and Chen-Yi Lee. 2020. Meta-rppg: Remote heart rate estimation using a transductive meta-learner. In *Computer Vision—ECCV 2020: 16th European Conference, Glasgow, UK, August 23–28, 2020, Proceedings, Part XXVII 16*. Springer, 392–409.
- [43] M Lewandowska et al. [n. d.]. Measuring Pulse Rate with a Webcam—a Non-contact Method for Evaluating Cardiac Activity; 2011. In *Proc. of the Federated Conf. on Computer Science and Information Systems*. 405–410.
- [44] Jianwei Li, Zitong Yu, and Jingang Shi. 2023. Learning motion-robust remote photoplethysmography through arbitrary resolution videos. In *Proceedings of the AAAI Conference on Artificial Intelligence*, Vol. 37. 1334–1342.
- [45] Xiaochen Li, Sicong Liu, Zimu Zhou, Bin Guo, Yuan Xu, and Zhiwen Yu. 2024. EchoPFL: Asynchronous Personalized Federated Learning on Mobile Devices with On-Demand Staleness Control. *Proceedings of the ACM on Interactive, Mobile, Wearable and Ubiquitous Technologies* 8, 1 (2024), 1–22.
- [46] Ji Lin, Chuang Gan, and Song Han. 2019. Tsm: Temporal shift module for efficient video understanding. In *Proceedings of the IEEE/CVF international conference on computer vision*. 7083–7093.
- [47] Sicong Liu, Junzhao Du, Kaiming Nan, Zimu Zhou, Hui Liu, Zhangyang Wang, and Yingyan Lin. 2020. AdaDeep: A usage-driven, automated deep model compression framework for enabling ubiquitous intelligent mobiles. *IEEE Transactions on Mobile Computing* 20, 12 (2020), 3282–3297.
- [48] Sicong Liu, Bin Guo, Ke Ma, Zhiwen Yu, and Junzhao Du. 2021. AdaSpring: Context-adaptive and runtime-evolutionary deep model compression for mobile applications. *Proceedings of the ACM on Interactive, Mobile, Wearable and Ubiquitous Technologies* 5, 1 (2021), 1–22.
- [49] Sicong Liu, Xiaochen Li, Zimu Zhou, Bin Guo, Meng Zhang, Haocheng Shen, and Zhiwen Yu. 2023. AdaEnlight: Energy-aware low-light video stream enhancement on mobile devices. *Proceedings of the ACM on Interactive, Mobile, Wearable and Ubiquitous Technologies* 6, 4 (2023), 1–26.
- [50] Xin Liu, Josh Fromm, Shwetak Patel, and Daniel McDuff. 2020. Multi-task temporal shift attention networks for on-device contactless vitals measurement. *Advances in Neural Information Processing Systems* 33 (2020), 19400–19411.
- [51] Xin Liu, Brian Hill, Ziheng Jiang, Shwetak Patel, and Daniel McDuff. 2023. Efficientphys: Enabling simple, fast and accurate camera-based cardiac measurement. In *Proceedings of the IEEE/CVF winter conference on applications of computer vision*. 5008–5017.
- [52] Xin Liu, Yuntao Wang, Sinan Xie, Xiaoyu Zhang, Zixian Ma, Daniel McDuff, and Shwetak Patel. 2022. Mobilephys: Personalized mobile camera-based contactless physiological sensing. *Proceedings of the ACM on Interactive, Mobile, Wearable and Ubiquitous Technologies* 6, 1 (2022), 1–23.
- [53] Yang Liu, Xiang Guo, and Yuzhong Zhang. 2024. Lightweight and interpretable convolutional neural network for real-time heart rate monitoring using low-cost video camera under realistic conditions. *Biomedical Signal Processing and Control* 87 (2024), 105461.
- [54] Hao Lu, Hu Han, and S Kevin Zhou. 2021. Dual-gan: Joint bvp and noise modeling for remote physiological measurement. In *Proceedings of the IEEE/CVF conference on computer vision and pattern recognition*. 12404–12413.
- [55] Daniel McDuff, Miah Wander, Xin Liu, Brian Hill, Javier Hernandez, Jonathan Lester, and Tadas Baltrusaitis. 2022. Scamps: Synthetics for camera measurement of physiological signals. *Advances in Neural Information Processing Systems* 35 (2022), 3744–3757.
- [56] J Moreno, J Ramos-Castro, J Movellan, E Parrado, G Rodas, and L Capdevila. 2015. Facial video-based photoplethysmography to detect HRV at rest. *International journal of sports medicine* (2015), 474–480.
- [57] Xuesong Niu, Hu Han, Shiguang Shan, and Xilin Chen. 2018. Synrhythm: Learning a deep heart rate estimator from general to specific. In *2018 24th international conference on pattern recognition (ICPR)*. IEEE, 3580–3585.
- [58] Xuesong Niu, Shiguang Shan, Hu Han, and Xilin Chen. 2019. Rhythmnet: End-to-end heart rate estimation from face via spatial-temporal representation. *IEEE Transactions on Image Processing* 29 (2019), 2409–2423.
- [59] Xuesong Niu, Zitong Yu, Hu Han, Xiaobai Li, Shiguang Shan, and Guoying Zhao. 2020. Video-based remote physiological measurement via cross-verified feature disentangling. In *Computer Vision—ECCV 2020: 16th European Conference, Glasgow, UK, August 23–28, 2020*,

- Proceedings, Part II 16*. Springer, 295–310.
- [60] Paolo Palatini and Stevo Julius. 1997. Heart rate and the cardiovascular risk. *Journal of hypertension* 15, 1 (1997), 3–17.
- [61] Olga Perepelkina, Mikhail Artemyev, Marina Churikova, and Mikhail Grinenko. 2020. HeartTrack: Convolutional neural network for remote video-based heart rate monitoring. In *Proceedings of the IEEE/CVF conference on computer vision and pattern recognition workshops*. 288–289.
- [62] Christian S Pilz, Sebastian Zaunseder, Jarek Krajewski, and Vladimir Blazek. 2018. Local group invariance for heart rate estimation from face videos in the wild. In *Proceedings of the IEEE conference on computer vision and pattern recognition workshops*. 1254–1262.
- [63] Ming-Zher Poh, Daniel J McDuff, and Rosalind W Picard. 2010. Advancements in noncontact, multiparameter physiological measurements using a webcam. *IEEE transactions on biomedical engineering* 58, 1 (2010), 7–11.
- [64] Ming-Zher Poh, Daniel J McDuff, and Rosalind W Picard. 2010. Non-contact, automated cardiac pulse measurements using video imaging and blind source separation. *Optics express* 18, 10 (2010), 10762–10774.
- [65] Rita Meziati Sabour, Yannick Benezeth, Pierre De Oliveira, Julien Chappe, and Fan Yang. 2021. Ubf-cphys: A multimodal database for psychophysiological studies of social stress. *IEEE Transactions on Affective Computing* 14, 1 (2021), 622–636.
- [66] Christopher G Scully, Jinseok Lee, Joseph Meyer, Alexander M Gorbach, Domhnall Granquist-Fraser, Yitzhak Mendelson, and Ki H Chon. 2011. Physiological parameter monitoring from optical recordings with a mobile phone. *IEEE Transactions on Biomedical Engineering* 59, 2 (2011), 303–306.
- [67] Sarah Ali Siddiqui, Yuan Zhang, Zhiqian Feng, and Anton Kos. 2016. A pulse rate estimation algorithm using PPG and smartphone camera. *Journal of medical systems* 40 (2016), 1–6.
- [68] Karan Singhal, Shekoofeh Azizi, Tao Tu, S Sara Mahdavi, Jason Wei, Hyung Won Chung, Nathan Scales, Ajay Tanwani, Heather Cole-Lewis, Stephen Pfohl, et al. 2023. Large language models encode clinical knowledge. *Nature* 620, 7972 (2023), 172–180.
- [69] Rencheng Song, Huan Chen, Juan Cheng, Chang Li, Yu Liu, and Xun Chen. 2021. PulseGAN: Learning to generate realistic pulse waveforms in remote photoplethysmography. *IEEE Journal of Biomedical and Health Informatics* 25, 5 (2021), 1373–1384.
- [70] Radim Špetlík, Vojtech Franc, and Jiri Matas. 2018. Visual heart rate estimation with convolutional neural network. In *Proceedings of the british machine vision conference, Newcastle, UK*. 3–6.
- [71] Zhaodong Sun, Alexander Vedernikov, Virpi-Liisa Kykyri, Mikko Pohjola, Miriam Nokia, and Xiaobai Li. 2022. Estimating stress in online meetings by remote physiological signal and behavioral features. In *Adjunct Proceedings of the 2022 ACM International Joint Conference on Pervasive and Ubiquitous Computing and the 2022 ACM International Symposium on Wearable Computers*. 216–220.
- [72] Duc Nhan Tran, Hyukzae Lee, and Changick Kim. 2015. A robust real time system for remote heart rate measurement via camera. In *2015 IEEE International Conference on Multimedia and Expo (ICME)*. IEEE, 1–6.
- [73] Gill R Tsouri, Survi Kyal, Sohail Dianat, and Lalit K Mestha. 2012. Constrained independent component analysis approach to nonobtrusive pulse rate measurements. *Journal of biomedical optics* 17, 7 (2012), 077011–077011.
- [74] Wim Verkruijsse, Lars O Svaasand, and J Stuart Nelson. 2008. Remote plethysmographic imaging using ambient light. *Optics express* 16, 26 (2008), 21434–21445.
- [75] Danyang Wang, Jianhao Weng, Yongpan Zou, and Kaishun Wu. 2022. EmoTracer: A Wearable Physiological and Psychological Monitoring System With Multi-modal Sensors. In *Adjunct Proceedings of the 2022 ACM International Joint Conference on Pervasive and Ubiquitous Computing and the 2022 ACM International Symposium on Wearable Computers*. 444–449.
- [76] Wenjin Wang, Albertus C Den Brinker, Sander Stuijk, and Gerard De Haan. 2016. Algorithmic principles of remote PPG. *IEEE Transactions on Biomedical Engineering* 64, 7 (2016), 1479–1491.
- [77] Zhen Wang, Yunhao Ba, Pradyumna Chari, Oyku Deniz Bozkurt, Gianna Brown, Parth Patwa, Niranjana Vaddi, Laleh Jalilian, and Achuta Kadambi. 2022. Synthetic generation of face videos with plethysmograph physiology. In *Proceedings of the IEEE/CVF conference on computer vision and pattern recognition*. 20587–20596.
- [78] Zhi-Kuan Wang, Ying Kao, and Chiou-Ting Hsu. 2019. Vision-based heart rate estimation via a two-stream cnn. In *2019 IEEE international conference on image processing (ICIP)*. IEEE, 3327–3331.
- [79] Bing Wei, Xuan He, Chao Zhang, and Xiaopei Wu. 2017. Non-contact, synchronous dynamic measurement of respiratory rate and heart rate based on dual sensitive regions. *Biomedical engineering online* 16 (2017), 1–21.
- [80] Hanguang Xiao, Tianqi Liu, Yisha Sun, Yulin Li, Shiyi Zhao, and Alberto Avolio. 2024. Remote photoplethysmography for heart rate measurement: A review. *Biomedical Signal Processing and Control* 88 (2024), 105608.
- [81] Honglin Xiong, Sheng Wang, Yitao Zhu, Zihao Zhao, Yuxiao Liu, Linlin Huang, Qian Wang, and Dinggang Shen. 2023. DoctorGlm: Fine-tuning your chinese doctor is not a herculean task. *arXiv preprint arXiv:2304.01097* (2023).
- [82] Zitong Yu, Xiaobai Li, Xuesong Niu, Jingang Shi, and Guoying Zhao. 2020. Autohr: A strong end-to-end baseline for remote heart rate measurement with neural searching. *IEEE Signal Processing Letters* 27 (2020), 1245–1249.
- [83] Zitong Yu, Xiaobai Li, and Guoying Zhao. 2019. Remote photoplethysmograph signal measurement from facial videos using spatio-temporal networks. *arXiv preprint arXiv:1905.02419* (2019).
- [84] Zitong Yu, Yuning Shen, Jingang Shi, Hengshuang Zhao, Philip HS Torr, and Guoying Zhao. 2022. Physformer: Facial video-based physiological measurement with temporal difference transformer. In *Proceedings of the IEEE/CVF conference on computer vision and*

pattern recognition. 4186–4196.

- [85] Tianfang Zhang, Cong Shi, Tianming Zhao, Zhengkun Ye, Payton Walker, Nitesh Saxena, Yan Wang, and Yingying Chen. 2022. Personalized health monitoring via vital sign measurements leveraging motion sensors on AR/VR headsets. In *Proceedings of the 20th Annual International Conference on Mobile Systems, Applications and Services*. 529–530.

A APPENDIX

A.1 Optical Principles

In Sec. 3.3, we provide the optical principles behind the differential frames, and here we give the detailed proof. The RGB values captured by the cameras is given by:

$$C_k(t) = I(t) \cdot (v_s(t) + v_d(t)) + v_n(t) \quad (4)$$

where $I(t)$ is the luminance intensity level, modulated by the specular reflection $v_s(t)$ and the diffuse reflection $v_d(t)$. The quantization noise of the camera sensor is captured by camera sensor is captured by $v_n(t)$. We can decompose $v_s(t)$ and $v_d(t)$ into stationary and time-dependent parts:

$$v_d(t) = u_d \cdot d_0 + u_p \cdot p(t) \quad (5)$$

where u_d is the unit color vector of the skin-tissue; d_0 is the stationary reflection strength; u_p is the relative pulsatile strengths caused by hemoglobin and melanin absorption; $p(t)$ represents the physiological changes.

$$v_s(t) = u_s \cdot (s_0 + \Phi(m(t), p(t))) \quad (6)$$

where u_s denotes the unit color vector of the light source spectrum; s_0 and $\Phi(m(t), p(t))$ denote the stationary and varying parts of specular reflections; $m(t)$ denotes all the non-physiological variations such as flickering of the light source, head rotation, and facial express.

Therefore, performing diff operations between adjacent video frames can quantify the optical changes caused by physiological or non-physiological components.

A.2 Network Structure

We propose fast long-range spatio-temporal heart rate recognizing module in 3.4. We provide some additional details on the specific implementation here.

- Incorporating Temporal Shift to 2D Convolution for Lightweight Spatio-temporal Modeling. There are two method to use temporal shift module: In-place shift and Residual shift. We use Residual shift as it can address the degraded spatial feature learning problem, as all the information in the original activation is still accessible after temporal shift through identity mapping.
- Network structure of multi-branch parallel spatio-temporal model. The computational process for the djacent frame branch and the segment branch is the same. The input data size is 3x36x36. Performing the first convolution operation, the output feature map size is 32x36x36. Performing the second convolution operation, the output feature map size is still 32x36x36. Then perform average pooling and Dropout operations, with a pooling kernel size of 2x2 and a stride of 2, the output feature map size is 32x18x18. Next, perform one convolution operation, the output feature map size is 32x18x18. Then perform another convolution operation, the output feature map size is 64x18x18. Finally, perform one average pooling and Dropout operation, with a pooling kernel size of 2x2 and a stride of 2, the output feature map size is 64x9x9.

A.3 Deployment

The CPUs of the 4 devices used in the experiments in 4 are all ARM architecture, so we take Device D_1 : Raspberry Pi 4B as an example to give the configuration required for deploying UbiHR. We use the official Raspberry Pi system and install the driver for the test camera as the basic environment and use virtualenv as the Python

environment management tool. The specific Python environment configuration is as follows: We run the program using Python 3.8.8, and use SciPy 1.8.0 and PyTorch 1.12 (CPU version) for network deployment and inference, and use OpenCV-Python 4.5.2 to process the video frames captured by the camera. The specific operations are as follows: First, please make sure that your device has completed the correct installation of the above environment and correctly set up the camera. Second, modifying the configuration file corresponding to UbiHR so that the system can correctly read the input video stream and save the output results. Third, please use the recorded video file to test UbiHR to ensure that the model can be read correctly and the system can run normally. Finally, please modify the system code to access the camera as real-time input. In addition, if necessary, you can configure the corresponding node.js and npm tools to draw the results in real time on a local web page.

When UbiHR is performing inference, we use the dstat tool to monitor and record the real-time hardware usage of the device, such as CPU and memory. As for the real-time inference results, we use the charting tools in JavaScript to plot the real-time heart rate results inferred by UbiHR and present them on the frontend interface.

Received 1 May 2024